Optical anisotropy of shaped oriented cobalt nanoparticles by generalized spectroscopic ellipsometry

M. Gilliot,* A. En Naciri,† and L. Johann
Université Paul Verlaine-Metz, Laboratoire de Physique des Milieux Denses, 1 Bd Arago, 57078 Metz Cedex 3, France

J. P. Stoquert, J. J. Grob, and D. Muller
Institut d'Electronique du Solide et des Systèmes, 23 rue du Loess, BP 20 CR, 67037 Strasbourg Cedex 2, France
(Received 1 February 2007; revised manuscript received 23 April 2007; published 26 July 2007)

We report on the application of generalized spectroscopic ellipsometry to the study of oriented prolate ellipsoidal cobalt nanoparticles embedded in a silica thin layer. The elongation of the cobalt particles with ellipsoidal form has been obtained by irradiation of spherical cobalt particles with swift heavy ions. Such a nanostructured medium constitutes an absorbing uniaxial medium with axis oriented 50° from the normal. The rotating polarizer ellipsometer with three elements has been extended to generalized ellipsometry and has been used to determine the anisotropic optical responses of the nanostructured layers. The technique we have developed is based on the acquisition of various spectra for different positions of the elements of the instrument and numerical extraction from these data of generalized ellipsometric parameters. The analysis of the sample is processed in three steps: development of an *a priori* model and simulation of the optical responses, acquisition of the experimental data and extraction of the generalized ellipsometric parameters, and, finally, numerical fitting of the model. Calculations of the anisotropic electromagnetic response are based on the Berreman formalism. The sample is represented by a stack of three sublayers on a silicon substrate: a top and bottom sublayer made of pure silica and an intermediate sublayer made of a mix of anisotropic cobalt particles and silica. The mix is represented by the generalized Maxwell-Garnett model that gives the effective dielectric constant of the nanostructured medium when this medium is supposed to be made of particles with a single kind of shape in a host medium. To improve our model, a different generalized Maxwell-Garnett formula has been developed to take two different kinds of shapes into account. This approximation has especially been used to represent a medium made of both spherical and ellipsoidal particles. It has been shown that the good agreement between calculated and experimental data can be improved using this different approach of generalized Maxwell-Garnett formula. Despite the complexity of the implanted anisotropic sample, our experimental method and models have lead, on the one hand, to the understanding of this complex anisotropic sample and, on the other hand, to the confident determination of various meaningful parameters that compose this optical response, such as the thicknesses of the sublayers, volume fraction, orientation, and shape factor of the cobalt particles.

DOI: 10.1103/PhysRevB.76.045424 PACS number(s): 36.40.Vz, 42.25.Dd, 42.25.Ja, 61.46.Bc

I. INTRODUCTION

Because of the increasing demand and needs in data storage density, magnetic nanoparticles have become a topic of great interest in fundamental and applied research. Cobalt (Co) clusters have attracted attention to their magnetic properties, which make them very interesting for potential applications in data storage.[1,2] Special attention has been paid to the evolution of magnetic properties with the cluster sizes and the superparamagnetic behavior.[3–14] This superparamagnetic behavior is a drawback occurring when the size of the particles is reduced, which makes the orientation of the magnetic moment of a particle unstable in time by the only effect of thermal agitation. The mean lifetime of an induced orientation is directly linked to anisotropy energy.[15,16] A way to change the anisotropy energy of particles is to change their shapes. Because of this, particles with nonspherical shapes are interesting objects to study. Co particles with spherical or nonspherical shapes have been studied for their magnetic or magneto-optical properties, but only a few studies have focused on their linear optical properties.[17–21] Knowledge and understanding of optical response is, however, of fundamental interest to completely understand the magneto-optical response of cobalt nanostructured layers.[22,23] That is one of the motivation that has brought us to study optical responses of cobalt nanostructured layers obtained by ion implantation of Co ions in a silica layer by spectroscopic ellipsometry.[24] In this paper, we propose an extension of this study to particles with ellipsoidal shapes thanks to the use of generalized spectroscopic ellipsometry.

Generalized ellipsometry is the measurement of diagonal and nondiagonal elements of the normalized Jones matrix of optically anisotropic samples. It has been shown to be very powerful for the characterization of anisotropic materials, allowing, with the help of models, the determination of optical constants, the lamellar structure, or composition of complex anisotropic samples. From the experimental point of view, this technique is, however, hardly manageable because the anisotropic effects are very low compared to the isotropic ones. It is also a theoretically challenging task involving many calculations and modeling processes. Because of this, for more than 20 years, generalized ellipsometry has become subject to large innovations, improvements, developments, and applications. Azzam and Bashara[25] have, for the first

time, made known the idea of generalized ellipsometry and proposed an extension of the null ellipsometer to generalized ellipsometry. Among all contributions to the development of this technique, Hauge[26] has used a rotating compensator ellipsometer to optically measure uniaxial anisotropic surfaces. More recently, Schubert *et al.* have used an extension of the rotating analyzer ellipsometer for the characterization of different kinds of anisotropic materials such as rutile TiO_2,[27] BN thin films,[28] liquid crystals,[29] monocrystalline $CdAl_2Se_4$ (Ref. 30) thin films, or $Al_{0.48}Ga_{0.52}InP_2$.[31] Infrared Fourier transform ellipsometer has also been used.[32–37] En Naciri *et al.* have used a Fourier analysis on a rotating polarizer ellipsometer to determine optical properties of HgI_2 uniaxial substrates.[38] Jellison and Modine have developed a double-modulation Mueller matrix ellipsometer[39,40] and used it to characterize different anisotropic materials such as TiO_2, $LiNbO_3$, or ZnO.[41–47] Lee *et al.*[48] have developed a rotating compensator ellipsometer allowing the measurement of the Stokes vector of the reflected light on a sample when the incident light is linearly polarized. They have used it for different applications on thin films.[49–52] They have also developed a doubly rotating compensator Mueller matrix ellipsometer[53–55] with applications on semiconductors or on sculptured thin films.[56–58] However, few works have been published about the use of generalized ellipsometry to investigate the optical reponses of anisotropic nanoparticles.[59,60]

In this paper, we report on a study of shaped oriented prolate ellipsoidal Co nanoparticles embedded in a silica thin layer by generalized spectroscopic ellipsometry. First, we give a short review of the principles of generalized ellipsometry and the analytical expression describing our experimental technique. Then a short description of the sample under study is given before we describe simulation procedures and experimental results. We also give the numerical procedure to determine the optical responses of the layers with embedded oriented prolate ellipsoidal Co nanoparticles and extract various parameters such as thicknesses of the layers, volume fraction, orientation, and shape factor of Co particles. Finally, we give in the Appendix details about the conventional and generalized Maxwell-Garnett models, and an extension of these formulas to take into account two different kinds of particle shapes.

II. GENERALIZED ELLIPSOMETRY AND MEASUREMENT TECHNIQUE

Because of the anisotropic morphology of the particles, the sample is expected to be optically anisotropic. The optical behavior of an anisotropic sample is described by its nondiagonal reflection Jones matrix R:

$$R = \begin{bmatrix} r_{pp} & r_{ps} \\ r_{sp} & r_{ss} \end{bmatrix}. \tag{1}$$

p refers to the linear state of polarization of light along the direction parallel to the plane of incidence and s refers to the linear state of polarization of light along the direction perpendicular to the plane of incidence. r_{pp} and r_{ss} are amplitude reflection coefficients from p (s) to p (s) polarization mode. They are isotropic components and they denote the part of reflected light corresponding to polarization mode conservation. r_{ps} and r_{sp} are amplitude reflection coefficients from s (p) to p (s) polarization mode. They are anisotropic components and they denote the part of reflected light which corresponds to polarization mode conversion. Anisotropic reflection coefficients have much lower amplitudes than isotropic ones. Generalized ellipsometry is the measurement of the generalized ellipsometric angles Ψ_{pp}, Ψ_{ps}, Ψ_{sp}, Δ_{pp}, Δ_{ps}, and Δ_{sp} linked to the Jones reflection matrix of the anisotropic sample:[61]

$$\rho_{pp} = \frac{r_{pp}}{r_{ss}} = \tan \Psi_{pp} e^{i\Delta_{pp}}, \tag{2}$$

$$\rho_{ps} = \frac{r_{ps}}{r_{ss}} = \tan \Psi_{ps} e^{i\Delta_{ps}}, \tag{3}$$

$$\rho_{sp} = \frac{r_{sp}}{r_{ss}} = \tan \Psi_{sp} e^{i\Delta_{sp}}. \tag{4}$$

The Ψ angles refer to amplitudes, whereas the Δ angles are phase changes of the ellipsometric ratios. These angles characterize the change of polarization state after reflection on the sample. They depend on different parameters such as thicknesses of the different layers making up the sample, complex refractive indices of each of these layers or dielectric tensors when materials are anisotropic, angle of incidence, and orientation of the sample. This measurement technique is information-rich, but it is indirect in a sense that measured quantities need to be compared or fitted to data generated from a model representing the sample. Note that when all materials composing the samples are isotropic, the anisotropic optical components vanish and the ellipsometric study reduces to the investigation of the Ψ and Δ conventional ellipsometric angles related to the ratio of the r_{pp} and r_{ss} isotropic reflection coefficients by[61]

$$\rho = \frac{r_{pp}}{r_{ss}} = \tan \Psi e^{i\Delta}. \tag{5}$$

As stated in the Introduction, there are different ways to carry out the measurement of generalized ellipsometric parameters. There is no ideal or standard generalized ellipsometric instrument, and the technique is still under progress and development. We have performed generalized ellipsometric measurements in the 350–850 nm spectral range at incident angle of 70° using a single-modulation solution. The instrument we have used is a rotating-polarizer-type ellipsometer. This instrument is shown in Fig. 1. The light emitted by a xenon source passes through a fixed polarizer and becomes linearly polarized. It then passes through a rotating polarizer, which provides a light intensity modulation before it is reflected by the sample, and finally analyzed. The light after being analyzed is collected and spectrally decomposed by a monochromator and changed to an electrical signal by a photomultiplier tube. The resulting signal is then computer processed. The signal representing the light intensity emerging from the analyzer has the following Fourier development expression:[62]

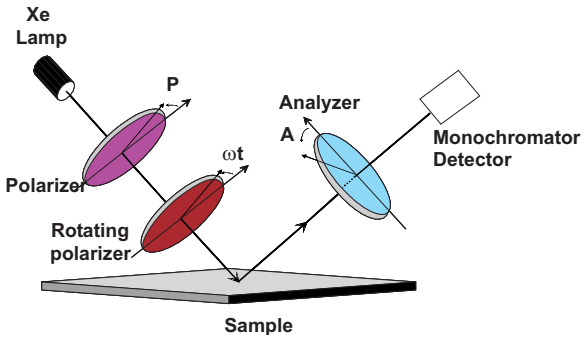

FIG. 1. (Color online) Schematic view of the rotating polarizer ellipsometer.

$$I = I_0[1 + a_{2c}\cos 2\omega t + a_{2s}\sin 2\omega t + a_{4c}\cos 4\omega t + a_{4s}\sin 4\omega t]. \quad (6)$$

The result of the electronic processing is the four Fourier coefficients. In the case of an anisotropic sample, these Fourier coefficients can be expressed by

$$a_{2c} = \frac{2(\alpha + \cos 2P)}{(2 + \alpha\cos 2P + \beta\sin 2P)}, \quad (7)$$

$$a_{2s} = \frac{2(\beta + \sin 2P)}{(2 + \alpha\cos 2P + \beta\sin 2P)}, \quad (8)$$

$$a_{4c} = \frac{(\alpha\cos 2P - \beta\sin 2P)}{(2 + \alpha\cos 2P + \beta\sin 2P)}, \quad (9)$$

$$a_{4s} = \frac{(\beta\cos 2P + \alpha\sin 2P)}{(2 + \alpha\cos 2P + \beta\sin 2P)}. \quad (10)$$

The α and β parameters depend on the generalized ellipsometric angles following:

$$\alpha = \frac{\alpha_1 - \alpha_2}{\alpha_1 + \alpha_2} \quad \text{and} \quad \beta = \frac{2\beta_1}{\alpha_1 + \alpha_2}, \quad (11)$$

with

$$\alpha_1 = \tan^2\psi_{pp} + \tan^2 A\tan^2\psi_{sp} + 2\tan A\tan\psi_{pp}\tan\psi_{sp}\cos(\Delta_{pp} - \Delta_{sp}), \quad (12)$$

$$\alpha_2 = \tan^2 A + \tan^2\psi_{ps} + 2\tan A\tan\psi_{ps}\cos\Delta_{ps}, \quad (13)$$

$$\beta_1 = \tan\psi_{pp}\tan\psi_{ps}\cos(\Delta_{pp} - \Delta_{ps}) + \tan A\tan\psi_{pp}\cos\Delta_{pp} + \tan A\tan\psi_{ps}\tan\psi_{sp}\cos(\Delta_{ps} - \Delta_{sp}) + \tan^2 A\tan\psi_{sp}\cos\Delta_{sp}. \quad (14)$$

The four Fourier coefficients a_{2c}, a_{2s}, a_{4c}, and a_{4s} are the experimental quantities resulting from one measurement. They depend on the analyzer azimuth A, on the fixed polarizer azimuth P, and on the generalized ellipsometric angles of the sample. In one set of measured Fourier coefficients, only the two α and β parameters contain useful information on the sample. Using the following notations:

$$x_1 = \tan^2\Psi_{pp}, \quad x_2 = \tan^2\Psi_{ps}, \quad x_3 = \tan^2\Psi_{sp}, \quad (15)$$

$$x_4 = \tan\Psi_{ps}\cos\Delta_{ps}, \quad x_5 = \tan\Psi_{sp}\cos\Delta_{sp}, \quad (16)$$

$$x_6 = \tan\Psi_{pp}\cos\Delta_{pp} + \tan\Psi_{ps}\tan\Psi_{sp}\cos(\Delta_{ps} - \Delta_{sp}), \quad (17)$$

$$x_7 = \tan\Psi_{pp}\tan\Psi_{sp}\cos(\Delta_{pp} - \Delta_{sp}), \quad (18)$$

$$x_8 = \tan\Psi_{pp}\tan\Psi_{ps}\cos(\Delta_{pp} - \Delta_{ps}), \quad (19)$$

it can be seen that the knowledge of one couple (α, β) leads to two linear equations:

$$(\alpha - 1)x_1 + (\alpha + 1)x_2 + (\alpha - 1)\tan^2 Ax_3 + 2(\alpha + 1)\tan Ax_4 + 2(\alpha - 1)\tan Ax_7 + (\alpha + 1)\tan^2 A = 0, \quad (20)$$

$$\beta x_1 + \beta x_2 + \beta\tan^2 Ax_3 + 2\beta\tan Ax_4 - 2\tan^2 Ax_5 - 2\tan Ax_6 + 2\beta\tan Ax_7 - 2x_8 + \beta\tan^2 A = 0. \quad (21)$$

Theoretically, one set of four measurements for different positions of the analyzer is enough to invert this system of linear equations and to determine these eight unknown parameters. However, because the anisotropic components are very low compared to the isotropic ones, anisotropic components can be shadowed by the noise of the isotropic ones. The analysis of the signal containing simultaneous contributions of isotropic and anisotropic components is delicate, and this inversion is not easy. To get round this limitation, we have chosen particular configurations of the instrument. A special configuration corresponds to the position of the analyzer $A = 90°$. This position allows the determination of the sp parameters, P being chosen as $P = 0°$ so that a maximum of incident light intensity is, on average, concentrated on the sp mode conversion rather than on the ss mode conservation. The second special configuration corresponds to the positions $P = 90°/A = 0°$, allowing the determination of the ps parameters. The two measurements corresponding to the positions $P = 45°/A = 45°$ and $P = 45°/A = -45°$ have then completed the set of measurements. The generalized ellipsometric parameters $\tan\Psi_{pp}$, $\tan\Psi_{ps}$, $\tan\Psi_{sp}$, $\cos\Delta_{pp}$, $\cos\Delta_{ps}$, and $\cos\Delta_{sp}$ are then extracted from the x_i parameters using relations (15)–(19). To reduce effects of experimental errors, especially in the 0° or 90° positions of the analyzer, which are critical measurement positions where detection errors are expected to have the most significant drawbacks, a set of 20 more spectra is used to determine an average value for the generalized ellipsometric parameters. The generalized ellipsometric parameters obtained by the four previous measurements are used as initial values to extract average values by minimizing, for each wavelength of the spectrum, the test function:

$$\chi^2 = \frac{1}{M}\sum_{i=1}^{M}[(a_{2c}^e - a_{2c}^c)^2 + (a_{2s}^e - a_{2s}^c)^2 + (a_{4c}^e - a_{4c}^c)^2 + (a_{4s}^e - a_{4s}^c)^2], \quad (22)$$

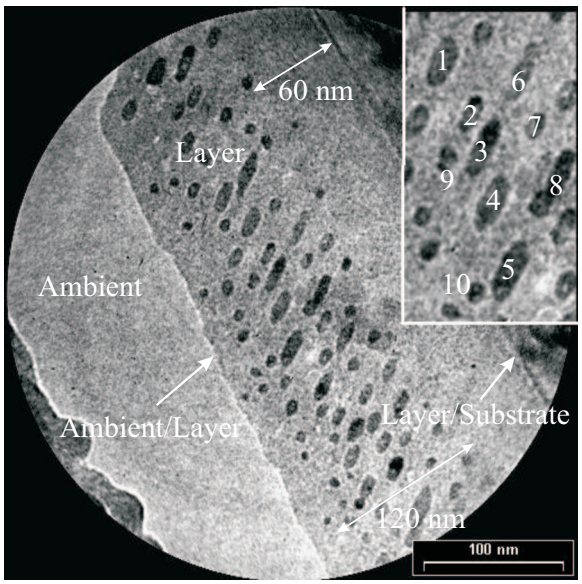

FIG. 2. (Color online) Transmission electron microscope image of the shaped particles.

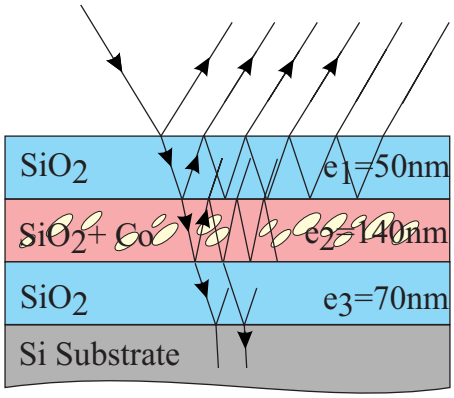

FIG. 3. (Color online) Three-layer model used for calculation of the optical response of the sample.

c denoting calculated coefficients as functions of the generalized ellipsometric parameters, e denoting the experimental coefficients, and M being the number of experimental spectra. The final results of this minimizing procedure are the generalized ellipsometric parameters $\tan \Psi_{pp}$, $\tan \Psi_{ps}$, $\tan \Psi_{sp}$, $\cos \Delta_{pp}$, $\cos \Delta_{ps}$, and $\cos \Delta_{sp}$ as a function of wavelength.

III. SAMPLE

The sample under investigation is made of oriented prolate ellipsoidal Co nanoparticles embedded in a silica thin layer. Such shape-oriented particles result in the irradiation of spherical particles with swift heavy ions, namely, 200 MeV I ions at a fluence of 5×10^{13} cm^{-2}, at room temperature with an incidence angle of 50°.[63–65] Spherical particles have previously been formed in a SiO_2 layer by implantation of Co ions at the energy of 160 keV and at fluence of 10^{17} cm^{-2} when the substrate temperature is maintained at 600 °C. It has been shown experimentally that irradiation of Co nanoparticles by swift heavy ions induces two separate regimes of size modification.[65] At low fluences, for particles smaller than a critical radius, particles grow but remain spherical, due to a fragmentation process followed by Ostwald ripening. At higher doses, prolate deformations are induced in the particles, with the major axis aligned with the beam direction. The deformation is attributed to the thermal spike responsible for the track formation along the trajectory of the incident ions. Transmission electron microscope (TEM) image of a slice of the sample after irradiation with I ions is shown in Fig. 2. The elongated shapes and the preferential orientation of the particles along the irradiation direction of the particles can be observed. In Table I, the ratio between length c and width a of the particles has been estimated from a transmission electron microscope image for a sample of ten particles. These particles are shown in the enlarged view in the inset of Fig. 2. The results show that the shape distribution of the particles is quite large.

IV. SIMULATION AND EXPERIMENTAL PROCEDURES

Such a sample with buried anisotropic nanoparticles has a complicated optical response. It is important to have an idea of this response so that favorable measurement configurations can be chosen. For this, the ellipsometric response of the sample has been simulated. The sample is represented by a stack of three sublayers: a pure silica top sublayer of 50 nm width, an intermediate sublayer of 140 nm width made of a mix of silica and Co nanostructures, and finally, a pure silica bottom sublayer of 70 nm width on the silicon substrate. The total thickness of the layer is fixed to 260 nm, which corresponds to the measured thickness of an unimplanted area of the sample. This structure and the thickness values are suggested by a previous study of spherical Co particles in silica layers. It has been shown that, from the optical point of view, nanoparticles are located in a 140 nm wide layer buried 50 nm beneath the sample surface.[24,66] The three sublayers can also be seen on the TEM image of Fig. 2, where the sample appears to be formed of three layers: a central sublayer rich in Co nanostructures, a bottom sublayer between the substrate and the particles, and finally, a top sublayer. The corresponding optical model used in our calculations is represented in Fig. 3.

The medium made by the mix of silica and the particles determines the anisotropic properties of the stack and needs to be described with care. In our model, all Co particles are

TABLE I. Ratio between the length c and width a of a sample of ten particles.

Particle number	1	2	3	4	5	6	7	8	9	10
c/a	2	2.25	2.8	2.33	2.5	2	1.75	2.8	1.4	1.25

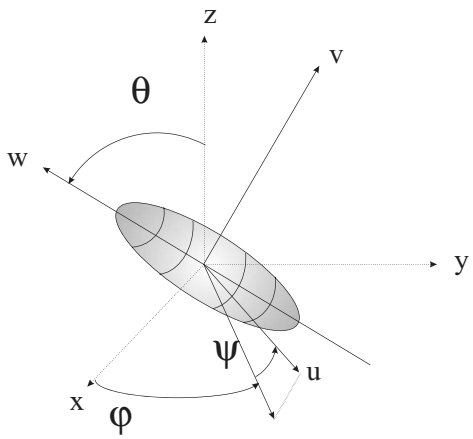

FIG. 4. Euler angles describing coordinate system change from the particle system to the laboratory system.

ellipsoidal and oriented along a particular axis. The relative orientation of these particles is a critical parameter directly linked to the anisotropic behavior of the sample. We use the Euler angles to describe the orientation of the particles as shown in Fig. 4. The system of axes (x,y,z) is related to the laboratory and the (u,v,w) one is related to the particles. The angle ψ indicates the rotation of the particles around their long axis. θ is assumed to be the angle of incidence of the irradiating beam, namely, 50°. φ can be changed by rotating the sample around the axis perpendicular to its surface. Since the particles are well separated, the medium made by the mix of silica and the particles can be considered as a generalized Maxwell-Garnett effective medium. The dielectric tensor in the particle coordinate systems of this medium is given by

$$\epsilon = \begin{pmatrix} \epsilon_u & 0 & 0 \\ 0 & \epsilon_u & 0 \\ 0 & 0 & \epsilon_w \end{pmatrix}, \tag{23}$$

where[67]

$$\frac{\epsilon_{u,w} - \epsilon_h}{L_{u,w}\epsilon_{u,w} + (1 - L_{u,w})\epsilon_h} = f\frac{\epsilon_i - \epsilon_h}{L_{u,w}\epsilon_i + (1 - L_{u,w})\epsilon_h}. \tag{24}$$

f is the volume fraction of the inclusions, and ϵ_i and ϵ_h are, respectively, the dielectric permittivity of the inclusions (cobalt) and the dielectric permittivity of the host medium (silica). $L_{u,w}$ are the shape factors of the particles in the direction u or w. They are linked by $2L_u + L_w = 1$. They can be calculated if the ratio between length c and width a of the axes of the particles is known.[68,69] These shape factors, as well as the orientation, are directly linked to the degree of anisotropy of the tensor.

Generalized Maxwell-Garnett approximation results in the application to ellipsoidal particles of a local field created by a cavity with the same shape as that of the particles. It assumes similar shapes, similar orientations, but possibly different volumes for all particles. Conditions required for the application of the Maxwell-Garnett approximation are nanospheres much smaller than the wavelength, so that their dipolar quasistatic representation is correct, and volume fraction that is not too high, so that particles are well separated and only dipolar interactions are taken into account. Maxwell-Garnett approximation is known to be valid for volume fractions around 10%, but Fu *et al.*[70] and Claro and Rojas[71] have proven this formula to be exact regardless of the particle concentration provided that the two-particle distribution is spherically symmetric. In our opinion, the applicability of the Maxwell-Garnett (MG) approximation only lies in the representation of the set of spheres by an equivalent homogeneously polarized medium. The applicability of MG is only a question of topology: the distribution of spheres has to be quite homogeneous and the clusters must be well separated with no aggregates. This is the case of the studied sample in this paper. It can be seen in Fig. 2 that no aggregates are formed, that the particles are well separated, and that the volume fraction estimated is not very high (around 5%, see Table II). More details about the derivation and meaning of this formula are given in the Appendix . Generalized Maxwell-Garnett model gives the effective dielectric constant of the mix in the coordinate system of the particles. The dielectric tensor in the laboratory coordinate systems $\epsilon_{x,y,z}$ is determined by applying Euler rotations to the dielectric tensor in the particle coordinate system $\epsilon_{u,v,w}$ according to

$$\epsilon_{x,y,z} = A\,\epsilon_{u,v,w}A^T, \tag{25}$$

where[72]

$$A = \begin{pmatrix} \cos\psi\cos\varphi - \cos\theta\sin\psi\sin\varphi & -\sin\psi\cos\varphi - \cos\theta\cos\psi\sin\varphi & \sin\theta\sin\varphi \\ \cos\psi\sin\varphi + \cos\theta\sin\psi\cos\varphi & -\sin\psi\sin\varphi + \cos\theta\cos\psi\cos\varphi & -\sin\theta\cos\varphi \\ \sin\theta\sin\psi & \sin\theta\cos\psi & \cos\theta \end{pmatrix}. \tag{26}$$

The complex dielectric tensor is diagonal in the particle coordinate system and it is nondiagonal but symmetrical in the laboratory coordinate system. This case occurs when the real part and the imaginary part of the complex dielectric tensor can be diagonalized in the same basis; i.e., when the principal refractive axis directions are the same as the principal absorption axis directions.[73]

By knowing the dielectric constant of the nanostructured layer, the optical response of the sample can be calculated, considering it as made up of three sublayers. The challenge

TABLE II. Summary of the numerical parameters used in our model: e_1 (thickness of the top layer), e_2 (thickness of the intermediate layer), e_3 (thickness of the bottom layer), f (volume fraction of inclusions), D (number of implanted atoms), L_w (shape factor of ellipsoidal particles), φ_0 (initial orientation angle), and χ^2 (fitting residue).

	e_1 (nm)	e_2 (nm)	e_3 (nm)	f	D (cm^{-2})	L_w	φ_0 (deg)	χ^2
Simulation starting point using generalized Maxwell-Garnett approximation	50	140	70	0.05	$6.4\ 10^{16}$	0.2	180	
Fit results using generalized Maxwell-Garnett approximation	76	116	47	0.053	$5.6\ 10^{16}$	0.16	174	0.65
Fit results using extended generalized Maxwell-Garnett approximation	71	128	42	0.048	$5.6\ 10^{16}$	0.15	175	0.55

in calculating such an optical response is to take into account interferences and multiple reflections including possible anisotropic effects at each interface of the stack, as shown schematically in Fig. 3. This can be done using the Berreman matrix formulation, describing electromagnetic waves in stratified anisotropic media.[61,74] Details and analytic solutions for the general case of biaxial media have been given by Schubert.[75] Based on these formulations, a calculation routine has been written to evaluate the optical response of our three layers on substrate model. Numerical values of the parameters used in this simulation are summarized in Table II. Shape factors and volume fraction used in this simulation are $L_w=0.2$ and $f=0.05$. The angle of incidence of the light beam on the sample is 70°. In our calculations, we have used bulk optical constants for nanostructured cobalt. This is valid for cobalt because we have not observed size effects.[24,66] The bulk approach works because of the poor free-electron behavior of cobalt in the considered spectral region. Maxwell-Garnett, generalized Maxwell-Garnett, and the extension we propose can be used for all kinds of materials. However, one should take care in using these models by taking into account possible size effects. These size effects can be introduced in the model by replacing the dielectric function for the inclusions ϵ_i with a size-dependent dielectric function for nanoscaled materials $\epsilon_i(c,a)$, including average size effect in both u and w directions of the particles. The simulated optical response of our model is given in Fig. 5 as $\tan\Psi_{pp}$, $\tan\Psi_{ps}$, $\tan\Psi_{sp}$, $\cos\Delta_{pp}$, $\cos\Delta_{ps}$, and $\cos\Delta_{sp}$ in the spectral range of 350–850 nm as a function of the orientation angle φ from −90° to 270°. It can be seen in this figure that the components $\tan\Psi_{pp}$, $\tan\Psi_{ps}$, $\tan\Psi_{sp}$, and $\cos\Delta_{pp}$ show a symmetrical behavior around the position $\varphi=90°$, while the parameters $\cos\Delta_{ps}$ and $\cos\Delta_{sp}$ show an antisymmetrical behavior around the position $\varphi=90°$. It can also be observed that the anisotropic components vanish in the particular orientation $\varphi=90°$, i.e., when the optical axis lies in the plane of incidence. This property of extinction of the components reflected on a uniaxial medium with its optical axis in the plane of incidence is known in the case of the reflection on a single anisotropic substrate[76] and in the case of the reflection on an anisotropic layer between two isotropic semi-infinite media.[77]

V. RESULTS AND DISCUSSION

These observations about the behavior of the simulated ellipsometric parameters as a function of the sample orientation φ show that an acquisition of three series of generalized ellipsometric parameters corresponding to three φ angles covering a range of 90° is a good choice for the characterization of our sample. From an arbitrary position φ_0 taken as the initial position, a first set of data has been acquired and the acquisition process repeated after the sample has then been rotated by 30° and again by 30°. Experimental results obtained by the method described in the previous section for these three positions are shown in Fig. 6 as scatter points. Note that all these spectra are characterized by a singularity around 400 nm attributed to an interference peak. In addition, it is seen that the anisotropic components are much weaker than the isotropic components. The obtained values as well as the behavior of generalized ellipsometric parameters $\tan\Psi_{pp}$, $\tan\Psi_{ps}$, $\tan\Psi_{sp}$, $\cos\Delta_{pp}$, $\cos\Delta_{ps}$, and $\cos\Delta_{sp}$ are in agreement with the results predicted by simulations shown in Fig. 5. The isotropic components $\tan\Psi_{pp}$ and $\cos\Delta_{pp}$ show little dependence on the sample rotation angle φ as predicted by these simulations. The same remark is valid for the sp anisotropic components, which characterize the conversion from p mode to s mode. An inversion of the curve in the $\cos\Delta_{ps}$ component is observed between the first measurement taken at $\varphi=\varphi_0$ and the following measurements where the sample is turned by 30°. Referring to the simulated curves, such an inversion of curve occurs around $\varphi=0°$ or $\varphi=180°$. This indicates that the selected arbitrary initial position corresponds, in fact, to an absolute position near 0° or 180°, i.e., $\varphi_0=0°$ or $\varphi_0=180°$. This assumption will be examined in the following.

Based on these experimental data, the calculated optical response of the sample can be adjusted by varying thickness, volume fraction, shape factor, and φ_0 in order to minimize the following test function:

$$\chi^2 = \frac{1}{N}\sum_{i=1}^{N}[(\tan\Psi_{pp}^e - \tan\Psi_{pp}^c)^2 + A(\tan\Psi_{ps}^e - \tan\Psi_{ps}^c)^2 + B(\tan\Psi_{sp}^e - \tan\Psi_{sp}^c)^2 + (\cos\Delta_{pp}^e - \cos\Delta_{pp}^c)^2 + (\cos\Delta_{ps}^e - \cos\Delta_{ps}^c)^2 + (\cos\Delta_{sp}^e - \cos\Delta_{sp}^c)^2]. \quad (27)$$

c denotes calculated coefficients, e denotes experimental coefficients, N is the number of spectral points, and A and B are factors that can be introduced so that, in the minimizing procedure, anisotropic components have the same weight as the

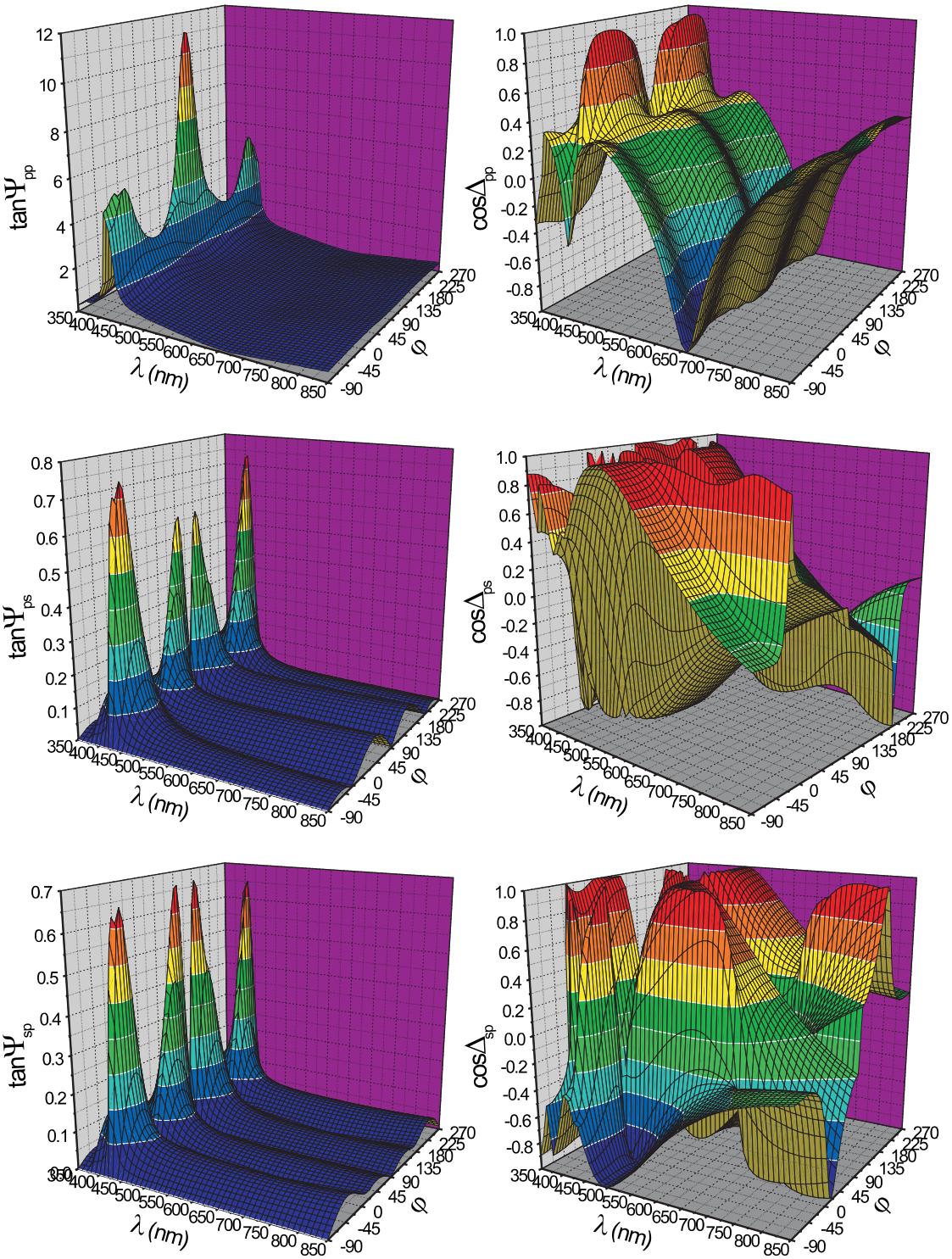

FIG. 5. (Color online) Simulation of the generalized ellipsometric parameters of a sample made of buried ellipsoidal Co nanoparticles as a function of the incident wavelength λ and of the orientation angle φ.

isotropic one. Fitting procedure is carried out simultaneously for the three orientation angles. Results obtained after minimization are shown in Fig. 6 as solid lines for the three φ azimuth positions. The result of the fitting procedure allows one to determine the volume fraction f of Co particles, the shape factor L_w, the thickness values e_1, e_2, and e_3 of the layers, and the initial orientation position φ_0. Numerical results for these parameters from this fitting procedure are summarized in Table II. The value of the average shape factor is $L_w=0.16$ and that of the volume fraction is $f=0.053$. The numerical results for the thicknesses are 76 nm for the top sublayer, 116 nm for the intermediate sublayer including the Co particles, and 47 nm for the bottom sublayer between the substrate and the structured sublayer. Thickness values

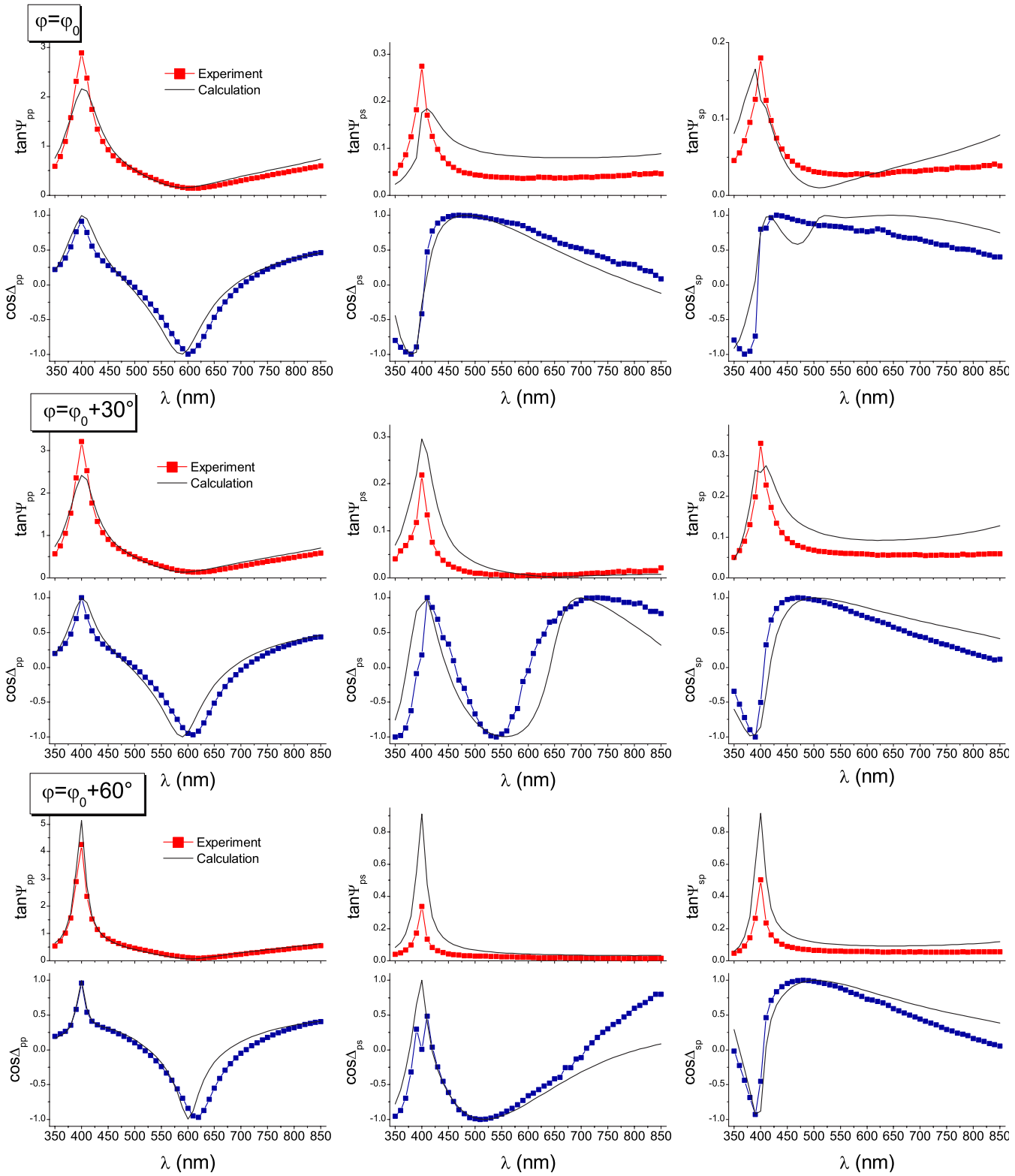

FIG. 6. (Color online) Experimental (points) and fitted (lines) generalized ellipsometric parameters of a sample made of buried ellipsoidal Co nanoparticles as a function of the incident wavelength λ using generalized Maxwell-Garnett approximation.

are in good agreement with what can be seen from the TEM image, except for the top sublayer which cannot be observed in the image because of the sample preparation for TEM observation that has damaged the top of the slice. On the whole, the shapes of the curves with their particular interference peaks are correctly reproduced, but small disagreements between experimental and calculated parameters can be observed. This disagreement appears essentially as an overestimate of the anisotropic components by the theory and a widening of the interference peak of the anisotropic components

which can be observed on $\tan \Psi_{ps}$ and $\tan \Psi_{sp}$. The curves of cosine components are well reproduced except the shape of $\cos \Delta_{sp}$ around 480 nm, in comparison to the experimental one. This can be explained by the following. The sample has been irradiated with heavy ions and many perturbing effects, especially large defects in silica, may have occurred, which are not included in the model. However, it has been shown in our previous study on spherical particles[24] that, because of the large domination of the particles in the optical response of cobalt nanostructured silica thin layers, silica defects are expected to have only a negligible contribution on the optical response of the sample. Although the defects in this sample may be different because of the use of swift heavy ions, we will assume that the same implantation mechanisms take place and we will suppose that defects only have little contribution and that the optical reponse is dominated by the contribution of the particles. Another drawback of our model which appears to be more critical is that it does not take into account the shape distribution of the particles.

Shapes of the particles are, indeed, introduced in the Maxwell-Garnett generalized approximation. It is based on the assumption of well-separated particles with all the same orientations and shapes, which, consequently, have all the same volume polarizability tensors. Differently shaped particles are characterized by different degrees of anisotropy. Our model accounts for an average shape anisotropy, whereas, as shown in the TEM image of Fig. 2 and Table I, the shapes in our sample are not all the same; especially, it contains a part of spherical particles. To take these particles into account, a different formula for generalized Maxwell-Garnett approximation has been derived considering two different shapes in the mix, which means two different polarizability tensors and two different local fields. We consider only two main populations of particles: spherical and ellipsoidal. This double possibility of geometries can be observed in the image of Fig. 2. Concerning the ellipsoidal particles, it can also be observed that there is a small dispersion in the ellipsoidal shape geometry. It is possible to build a model taking this little dispersion of the ellipsoidal shapes into account. This is, however, not our purpose because optical waves which have wavelengths much larger than the particles may not be sensitive to small fluctuations of the particle shape distribution function. Our formula for generalized Maxwell-Garnett approximation is denoted as extended generalized Maxwell-Garnett approximation. It is, first of all, based on a simple understanding of conventional Maxwell-Garnett approximation and then of generalized Maxwell-Garnett approximation. Basically, it is derived considering a local field on a particle that depends on the local geometry around the considered particle. This local field is calculated by assuming a cavity with the same shape as the considered particle. Details about the derivation of conventional Maxwell-Garnett approximation, generalized Maxwell-Garnett approximation for one shape, and our two-shape particle extended generalized Maxwell-Garnett formula are given in the Appendix . Assuming that both kinds of particles have the same orientation, the components of the dielectric tensor mentioned by Eq. (23) in the particle coordinate system (see Fig. 4) of this medium are given by

$$\epsilon_{u,w} = \epsilon_h + \eta\epsilon_h \frac{f_1(1+\eta L_{2,u,w}) + f_2(1+\eta L_{1,u,w})}{1+\eta[L_{1,u,w}(1-f_1) + L_{2,u,w}(1-f_2)] + \eta^2 L_{1,u,w}L_{2,u,w}(1-f_1-f_2)}, \tag{28}$$

with

$$\eta = \frac{\epsilon_i - \epsilon_h}{\epsilon_h}. \tag{29}$$

f_1 (f_2) is the volume fraction of the inclusions of type 1 (2), and ϵ_i and ϵ_h are, respectively, the dielectric permittivity of the inclusions (cobalt) and the dielectric permittivity of the host medium (silica). $L_{1,u,w}$ ($L_{2,u,w}$) are the shape factors of the particles of type 1 (2) in the direction u or w. The fitting procedure has been extended, taking the two-shape distribution of particles into account. The optical response of our model is adjusted to experimental data simultaneously for the three orientation angles when thicknesses, volume fractions of both kinds of particles, shape factor of particles of type 1, and φ_0 angle can be fitted by minimizing the test function Eq. (27). Shape factors of particles of type 2 are fixed to 0.33, which corresponds to spherical particles. Results obtained after minimization are shown in Fig. 7 as solid lines for the three azimuth positions. Agreement between theory and experiment is better at that time, especially, the amplitudes in the peaks of the anisotropic components are better respected. This improvement is appreciated by the χ^2 quality factor, which evolves from 0.65 to 0.55 when two shapes are accounted. Numerical results from this fitting procedure are summarized in Table II. The numerical results for the thicknesses are 71 nm for the top sublayer, 128 nm for the intermediate sublayer including the Co particles, and 42 nm for the bottom sublayer between the substrate and the particles. Thickness values are also in good agreement with what can be seen on TEM image and allow are to perfectly distinguish the nanostructured layer. Furthermore, the unimplanted part of the sample has been measured to a thickness value of 260 nm, whereas, according to the three-layer model, the implanted one is estimated to be 240 nm. The difference between implanted and unimplanted thicknesses is not surprising and must be the result of the sputtering phenomenon. These thickness values indicate a contraction of 20 nm of the central sublayer containing the Co particles as

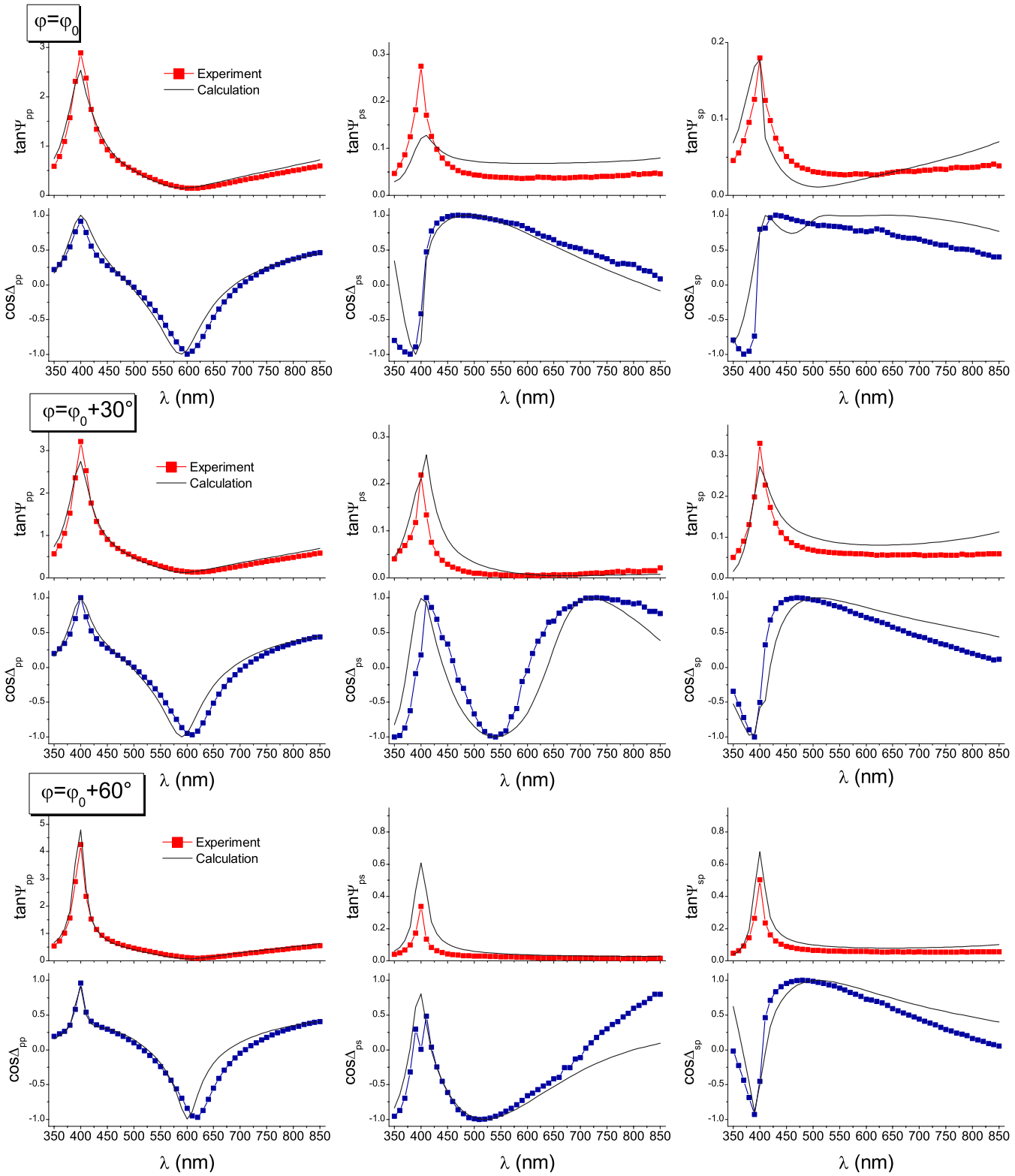

FIG. 7. (Color online) Experimental (points) and fitted (lines) generalized ellipsometric parameters of a sample made of burried ellipsoidal Co nanoparticles as a function of the incident wavelength λ assuming two different shapes of particles.

well as a displacement of this layer toward the substrate. This is brought about by the stronger irradiation by the heavy ions. It can also be noted that the volume fraction of $f_2=0.041$ for ellipsoidal particles and of $f_1=0.007$ for spherical particles, which make a total volume fraction for particles of $f=0.048$, lead to a total amount of 5.6×10^{16} Co/cm^2 in the sample. The initial sample position obtained after fitting is $\varphi_0=175°$, i.e., near 180°. Finally, the obtained shape factor is $L_w=0.16$, corresponding to a ratio c/a of the axis lengths of the ellipsoid of 2.2.[68] According to the TEM image of Fig. 2

and Table I, the shape factor value of 2.2 corresponds to the largest Co particles.

VI. CONCLUSION

The use of the rotating polarizer ellipsometer with three elements (fixed polarizer, rotating polarizer, and fixed analyzer) has been extended to generalized ellipsometry, which applies to optically anisotropic samples. Experimental data consisting of Fourier coefficients are numerically treated to extract the generalized ellipsometric parameters of Co nanoparticles with ellipsoidal shapes burried in silica. Such shaped particles have been obtained after irradiation by swift heavy ions, which elongates the particles in the irradiation direction. The sample has been represented by a three-sublayer structure: a top silica sublayer, an intermediate sublayer made of a mixture of silica and Co ellipsoidal particles, and a bottom sublayer of silica on the silicon substrate. The mixture of the anisotropic Co particles and silica can be represented by an effective medium based on the model of generalized Maxwell-Garnett approximation. In this model, the particles are characterized by their shape factors, which determine the anisotropy degree of the sample. The optical properties of such a medium are analyzed for different positions of the optical axis when the sample is rotated around the axis perpendicular to its surface. Electromagnetic responses of the model are calculated within the Berreman formalism framework. Good agreement between the experimental and predicted spectra has been obtained by this method. Various parameters have been determined, such as the thicknesses of the sublayers, the volume fraction of the Co particles, the orientation of the sample, and the average shape factor of the particles, which reveal that the optical response is dominated by the largest particles. Our model has then been improved by extending the generalized Maxwell-Garnett formula to a distribution of two kinds of particles characterized by two different shapes. This especially allows one to take into account the fraction of the particles that have not been modified by irradiation and which are still spherical in shape. The fit is not perfect because of the complexity of the studied implanted anisotropic sample, but good agreement has been obtained, taking into account subtle effects such as an optically anisotropic two-shape distribution of nanostructures in a layered structure.

APPENDIX: MAXWELL-GARNETT APPROXIMATION AND EXTENSIONS

We provide here a simple explanation of the well-known Maxwell-Garnett approximation. We give a derivation based on elementary ideas. This derivation is then extended to the generalized Maxwell-Garnett approximation describing dielectric permittivity of medium made up of ellipsoidal particles with identical shapes and orientations. Based on these calculations for deriving the conventional and generalized Maxwell-Garnett formulas, an extended version of the generalized Maxwell-Garnett formula is developed to calculate the dielectric permittivity of a mix consisting of particles with two kinds of shapes made of the same material in a host medium. We consider sizes of the particles much smaller than the incident wavelength so that the quasistatic approach is valid. The host medium is considered as the reference medium so that, in our electrostatic calculations, the dielectric permittivity of vacuum is replaced by the dielectric permittivity of the host medium. International System of units and notations are used.

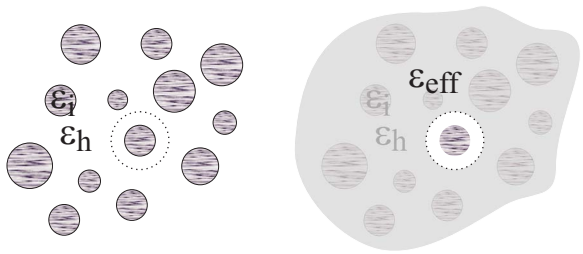

FIG. 8. (Color online) Maxwell-Garnett situation: (left) real configuration and (right) Lorentz calculation.

1. Conventional Maxwell-Garnett approximation

Considering a nanostructured medium made up of a set of spherical inclusions embedded in a host medium, Maxwell-Garnett approximation is a fine way to calculate interactions between the inclusions and especially to calculate the local field on a given particle due to the action of the other particles. An isolated particle of dielectric permittivity ϵ_i and volume v embedded in a host medium of dielectric permittivity ϵ_h submitted to an incident electric field $\vec{E}^I$ is polarized according to the dipole moment:

$$\vec{p} = \alpha \vec{E}^I, \tag{A1}$$

with[78]

$$\alpha = v\epsilon_h \beta, \tag{A2}$$

where

$$\beta = 3\frac{\epsilon_i - \epsilon_h}{\epsilon_i + 2\epsilon_h}. \tag{A3}$$

In nanostructured media consisting of a set of particles in a host medium, particles are interacting. The incident field on a given particle is then the superposition of the field created by external sources and the field radiated by the particles around the considered particle. An approximation to calculate the interaction field between the particles is the Lorentz local field. By considering one particle in the medium, the local field on it is calculated by replacing the action of the surrounding particles with the action of an equivalent effective medium around a spherical cavity centered on the considered particle as represented in Fig. 8. The macroscopic field $\vec{E}^M$ in the effective medium polarizes this effective medium with the volume polarization $\vec{P}$:

$$\vec{P} = (\epsilon_{\text{eff}} - \epsilon_h)\vec{E}^M. \tag{A4}$$

Due to this polarization in the effective medium, a surface charge density appears at the surface of the cavity. The field

$\vec{E}^S$ within the cavity caused by this surface charge is then given by the Lorentz local field:[79,80]

$$\vec{E}^S = \frac{\vec{P}}{3\epsilon_h}. \tag{A5}$$

The resulting incident field polarizing the particle within the cavity is the sum of the macroscopic field and this cavity field:

$$\vec{E}^I = \vec{E}^M + \frac{\vec{P}}{3\epsilon_h}. \tag{A6}$$

Inserting the polarizing incident field (A6) into the dipole moment (A1), we get the dipole moment of this particle. The dipole moment density vector is the volume average over all dipole moments, i.e., over all particles of the nanostructured medium:

$$\vec{P} = \frac{1}{V}\sum \vec{p} = f\beta\epsilon_h\vec{E}^I, \tag{A7}$$

where V is the volume of the medium and f is the volume fraction filled by the particles. Remaining that, finally, the effective dielectric constant is defined as $\vec{P}=(\epsilon_{eff}-\epsilon_h)\vec{E}^M$, we find the Maxwell-Garnett formula:

$$\epsilon_{eff} = \epsilon_h + \frac{f\beta\epsilon_h}{1-\frac{1}{3}f\beta}, \tag{A8}$$

or, written in another way,

$$\frac{\epsilon_{eff}-\epsilon_h}{\epsilon_{eff}+2\epsilon_h} = f\frac{\epsilon_i-\epsilon_h}{\epsilon_i+2\epsilon_h}. \tag{A9}$$

This formula expresses the dielectric constant ϵ_{eff} of the nanostructured medium made up of a set of inclusions embedded in a host medium. It is given here for one type of inclusions in the host medium, but it can generally be given for different kinds of spherical inclusions.[67,81]

2. Generalized Maxwell-Garnett approximation

In the case of ellipsoidal particles, these equations can be generalized to determine the effective dielectric tensor of a set of ellipsoidal particles having identical shapes and orientations but which can have different sizes, as represented in the right part of Fig. 9. Let us first consider an isolated ellipsoidal particle of volume v with axis directions u, v, and w as represented in Fig. 4. It has an isotropic dielectric permittivity ϵ_i and it is embedded in a host medium of dielectric permittivity ϵ_h. Submitted to an incident external electric field $\vec{E}^I$, this particle can be polarized according to the polarizability tensor $\tilde{\alpha}$ defined by[82]

$$\tilde{\alpha} = \begin{pmatrix} \alpha_u & 0 & 0 \\ 0 & \alpha_v & 0 \\ 0 & 0 & \alpha_w \end{pmatrix}, \tag{A10}$$

with

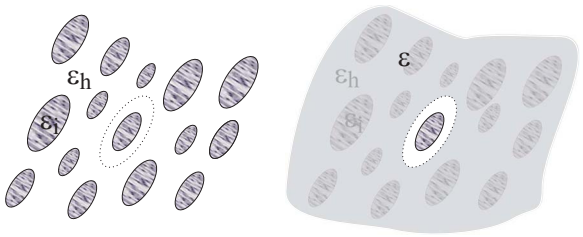

FIG. 9. (Color online) Generalized Maxwell-Garnett situation: (left) real configuration and (right) Lorentz calculation.

$$\alpha_{u,v,w} = v\epsilon_h\beta_{u,v,w}, \tag{A11}$$

where

$$\beta_{u,v,w} = \frac{\epsilon_i-\epsilon_h}{\epsilon_h+(\epsilon_i-\epsilon_h)L_{u,v,w}}. \tag{A12}$$

$L_{u,v,w}$ are the shape factors of the particles in the direction u, v, or w. The shape factors depend on the axis lengths of the ellipsoid.[68,69] They are directly linked to the degree of anisotropy of the tensor. Considering now nanostructured media made up of a set of ellipsoidal particles in interaction, generalized Maxwell-Garnett approximation consists in calculating the local field on a particle with replacing the actions of the surrounding particles by the action of an equivalent effective medium around a cavity with the same shape as that of the considered particle, as represented in the right part of Fig. 9. The local field $\vec{E}^I$ incident on the considered particle results in the superposition of the macroscopic field $\vec{E}^M$ and the field $\vec{E}^S$ caused by the surface charge at the interface between this cavity and the host medium. The components of the local field in the three u, v, and w directions are given by[80]

$$E^I_{u,v,w} = E^M_{u,v,w} + \frac{L_{u,v,w}P_{u,v,w}}{\epsilon_h}. \tag{A13}$$

$P_{u,v,w}$ are the three components of the average volume dipole moment $\vec{P}$. This volume dipole moment is calculated considering all dipoles, i.e., all particles in the volume V. Considering this local field (A13) as the polarizing field, we get the dipole moments $\vec{p}$ of all the particles and the average volume dipole moment, the components of which are calculated as

$$P_{u,v,w} = \frac{1}{V}\sum p_{u,v,w} = f\beta_{u,v,w}\epsilon_h E^I_{u,v,w}. \tag{A14}$$

Remaining that, finally, the effective dielectric tensor $\tilde{\epsilon}_{eff}$ is defined by

$$\vec{P} = (\tilde{\epsilon}_{eff}-\epsilon_h\tilde{I})\vec{E}^M, \tag{A15}$$

where $\tilde{I}$ is the identity tensor, we find the generalized Maxwell-Garnett formula in the particle coordinate systems:[67]

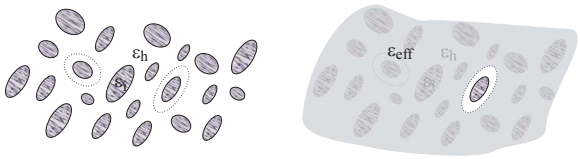

FIG. 10. (Color online) Extended generalized Maxwell-Garnett situation: (left) real configuration and (right) Lorentz calculation.

$$\tilde{\epsilon}_{eff} = \begin{pmatrix} \epsilon_u & 0 & 0 \\ 0 & \epsilon_v & 0 \\ 0 & 0 & \epsilon_w \end{pmatrix}, \tag{A16}$$

where

$$\epsilon_{u,v,w} = \epsilon_h + \frac{f\beta\epsilon_h}{1 - f\beta L_{u,v,w}}, \tag{A17}$$

or, written in another way,

$$\frac{\epsilon_{u,v,w} - \epsilon_h}{L_{u,v,w}\epsilon_{u,v,w} + (1 - L_{u,v,w})\epsilon_h} = f\frac{\epsilon_i - \epsilon_h}{L_{u,v,w}\epsilon_i + (1 - L_{u,v,w})\epsilon_h}. \tag{A18}$$

3. Extended generalized Maxwell-Garnett approximation

We consider now a mix made up of two kinds of particles characterized by two different shapes in the embedding host medium. All particles have identical orientations as represented in Fig. 10. They all have either a shape of type 1 or a shape of type 2, but they can have various volumes. The two kinds of particles have two different polarizability tensors $\tilde{\alpha}_1$ and $\tilde{\alpha}_2$ as given by Eq. (A11) linked to the two β_1 and β_2 factors as given by Eq. (A12) for the two shape factors $L_{1,u,v,w}$ and $L_{2,u,v,w}$. As in Maxwell-Garnett and generalized Maxwell-Garnett approximations, the local field on a particle is calculated by replacing the action of the surrounding particles with the action of an equivalent effective medium around a cavity with the same shape as that of the considered particle, as represented in the right part of Fig. 10. Here, one needs to consider two different local fields incident on the two kinds of shaped particles, $\vec{E}_1^I$ and $\vec{E}_2^I$, the components of which are given by[80]

$$E^I_{1,u,v,w} = E^M_{u,v,w} + \frac{L_{1,u,v,w}}{\epsilon_h} P_{u,v,w}, \tag{A19}$$

$$E^I_{2,u,v,w} = E^M_{u,v,w} + \frac{L_{2,u,v,w}}{\epsilon_h} P_{u,v,w}, \tag{A20}$$

respectively, for particles of type 1 and type 2. The volume polarization along the different directions is the volume average over all dipole moments in the volume V:

$$P_{u,v,w} = \frac{1}{V}\sum p_{1,u,v,w} + p_{2,u,v,w} = f_1\beta_{1,u,v,w}\epsilon_h E^I_{1,u,v,w} + f_2\beta_{2,u,v,w}\epsilon_h E^I_{2,u,v,w}. \tag{A21}$$

f_1 and f_2 are the volume fractions respectively, filled by the particles of type 1 and 2. Remaining $\vec{P} = (\tilde{\epsilon}_{eff} - \epsilon_h\tilde{I})\vec{E}^M$, we get, after a little algebra, the extended generalized Maxwell-Garnett effective dielectric tensor $\tilde{\epsilon}_{eff}$ the components of which are given by

$$\epsilon_{u,v,w} = \epsilon_h + \epsilon_h \frac{f_1\beta_1 + f_2\beta_2}{1 - f_1\beta_1 L_{1,u,v,w} - f_2\beta_2 L_{2,u,v,w}}, \tag{A22}$$

or, written in another way,

$$\epsilon_{u,v,w} = \epsilon_h + \eta\epsilon_h \frac{f_1(1 + \eta L_{2,u,v,w}) + f_2(1 + \eta L_{1,u,v,w})}{1 + \eta[L_{1,u,v,w}(1 - f_1) + L_{2,u,v,w}(1 - f_2)] + \eta^2 L_{1,u,v,w}L_{2,u,v,w}(1 - f_1 - f_2)}, \tag{A23}$$

with

$$\eta = \frac{\epsilon_i - \epsilon_h}{\epsilon_h}. \tag{A24}$$

*Electronic address: gilliot@univ-metz.fr
†Electronic address: ennacir@univ-metz.fr

[1] S. A. M. Tofail, I. Z. Rahman, and M. A. Rahman, Appl. Organomet. Chem. **15**, 373 (2001).
[2] N. Weiss, T. Cren, M. Epple, S. Rusponi, G. Baudot, S. Rohart, A. Tejeda, V. Repain, S. Rousset, P. Ohresser *et al.*, Phys. Rev. Lett. **95**, 157204 (2005).
[3] L. G. Jacobsohn, M. E. Hawley, D. W. Cooke, M. F. Hundley, J. D. Thompson, R. K. Schulze, and M. Nastasi, J. Appl. Phys. **96**, 4444 (2004).
[4] O. Cíntora-González, D. Muller, C. Estournès, M. Richard-Plouet, R. Poinsot, J. J. Grob, and J. Guille, Nucl. Instrum. Methods Phys. Res. B **178**, 144 (2001).
[5] C. D'Orléans, C. Cerruti, C. Estournès, J. J. Grob, J. L. Guille, F. Haas, D. Muller, M. Richard-Plouet, and J. P. Stoquert, Nucl. Instrum. Methods Phys. Res. B **209**, 316 (2003).
[6] D. H. Kim, J. S. Yang, Y. S. Kim, D.-W. Kim, T. W. Noh, S. D. Bu, Y.-W. Kim, Y. D. Park, S. J. Pearton, Y. Jo *et al.*, Appl.

Phys. Lett. **83**, 4574 (2003).
[7] E. Cattaruzza, F. Gonella, G. Mattei, P. Mazzoldi, D. Gatteschi, C. Sangregorio, M. Falconieri, G. Salvetti, and G. Battaglin, Appl. Phys. Lett. **73**, 1176 (1998).
[8] X. Xu, S. Yin, R. Moro, and W. A. de Heer, Phys. Rev. Lett. **95**, 237209 (2005).
[9] L. M. Socolovsky, C. L. P. Oliveira, J. C. Denardin, M. Knobel, and I. L. Torriani, Phys. Rev. B **72**, 184423 (2005).
[10] S. P. Gubin, Y. I. Spichkin, Y. A. Koksharov, G. Y. Yurkov, A. V. Kozinkin, T. I. Nedoseikina, M. S. Korobov, and A. M. Tishin, J. Magn. Magn. Mater. **265**, 234 (2003).
[11] Y. Huttel, H. Gómez, C. Clavero, A. Cebollada, G. Armelles, E. Navarro, M. Ciria, L. Benito, J. I. Arnaudas, and A. J. Kellock, J. Appl. Phys. **96**, 1666 (2004).
[12] S. Sun and C. B. Murray, J. Appl. Phys. **85**, 4325 (1999).
[13] C. Petit, A. Taleb, and M.-P. Pileni, Adv. Mater. (Weinheim, Ger.) **10**, 259 (1998).
[14] A. K. Pradhan, D. Hunter, J. B. Dadson, T. M. Williams, K. Zhang, K. Lord, B. Lasley, R. R. Rakhimov, J. Zhang, D. J. Sellmyer *et al.*, Appl. Phys. Lett. **86**, 222503 (2005).
[15] C. de Julián Fernández, G. Mattei, C. Sangregorio, C. Battaglin, D. Gatteschi, and P. Mazzoldi, J. Magn. Magn. Mater. **272-276**, E1235 (2004).
[16] W. Kuch, Nat. Mater. **2**, 505 (2003).
[17] J. Roiz, A. Oliver, E. Muñoz, L. Rodríguez-Fernández, J. M. Hernández, and J. C. Cheang-Wong, J. Appl. Phys. **95**, 1783 (2004).
[18] A. Duran, J. M. Fernandez Navarro, P. Casariego, and A. Joglar, J. Non-Cryst. Solids **82**, 391 (1986).
[19] G. A. Niklasson and C. G. Granqvist, J. Appl. Phys. **55**, 3382 (1984).
[20] G. A. Niklasson and C. G. Granqvist, Appl. Phys. Lett. **41**, 773 (1982).
[21] G. A. Niklasson, J. Appl. Phys. **57**, 157 (1985).
[22] B. Kalska, K. Schwinge, J. Paggel, P. Fumagalli, M. Hilgendorff, and M. Giersig, J. Appl. Phys. **98**, 044318 (2005).
[23] R. Carey, D. M. Newman, and B. W. J. Thomas, Thin Solid Films **129**, 231 (1985).
[24] M. Gilliot, A. E. Naciri, L. Johann, J. P. Stoquert, J. J. Grob, D. Muller, and M. Stchakovsky, Phys. Rev. B **74**, 045423 (2006).
[25] R. M. A. Azzam and N. M. Bashara, J. Opt. Soc. Am. **62**, 1521 (1972).
[26] P. S. Hauge, Surf. Sci. **56**, 148 (1976).
[27] M. Schubert, B. Rheinländer, J. A. Woollam, B. Johs, and C. M. Herzinger, J. Opt. Soc. Am. A **13**, 875 (1996).
[28] M. Schubert, B. Rheinländer, E. Franke, H. Neumann, J. Hahn, M. Röder, and F. Richter, Appl. Phys. Lett. **70**, 1819 (1997).
[29] M. Schubert, B. Rheinländer, C. Cramer, H. Schmiedel, J. A. Woollam, C. M. Herzinger, and B. Johs, J. Opt. Soc. Am. A **13**, 1930 (1996).
[30] J.-D. Hecht, A. Eifler, V. Riede, M. Schubert, G. Krauss, and V. Krämer, Phys. Rev. B **57**, 7037 (1998).
[31] M. Schubert, T. Hofmann, B. Rheinländer, I. Pietzonka, T. Sass, V. Gottschalch, and J. A. Woollam, Phys. Rev. B **60**, 16618 (1999).
[32] T. Hofmann, V. Gottschalch, and M. Schubert, Phys. Rev. B **66**, 195204 (2002).
[33] T. Hofmann, M. Schubert, and V. Gottschalch, Thin Solid Films **455-456**, 601 (2004).
[34] T. Hofmann, M. Schubert, C. M. Herzinger, and I. Pietzonka, Appl. Phys. Lett. **82**, 3463 (2003).
[35] M. Schubert, T. Hofmann, and C. M. Herzinger, Thin Solid Films **455-456**, 563 (2004).
[36] D. W. Thompson, M. J. DeVries, T. E. Tiwald, and J. A. Woollam, Thin Solid Films **313-314**, 341 (1998).
[37] C. Bundesmann, N. Ashkenov, M. Schubert, A. Rahm, H. v. Wenckstern, E. M. Kaidashev, M. Lorenz, and M. Grundmann, Thin Solid Films **455-456**, 161 (2004).
[38] A. En Naciri, L. Johann, and R. Kleim, Appl. Opt. **38**, 4802 (1999).
[39] G. E. Jellison and F. A. Modine, Appl. Opt. **36**, 8184 (1997).
[40] G. E. Jellison and F. A. Modine, Appl. Opt. **36**, 8190 (1997).
[41] G. E. Jellison, Jr., F. A. Modine, and L. A. Boatner, Opt. Lett. **22**, 1808 (1997).
[42] G. E. Jellison, Jr., J. O. Ramey, and L. A. Boatner, Phys. Rev. B **59**, 9718 (1999).
[43] G. E. Jellison, Jr. and L. A. Boatner, Phys. Rev. B **58**, 3586 (1998).
[44] G. E. Jellison, Jr. and L. A. Boatner, Phys. Rev. B **65**, 049902(E) (2001).
[45] G. E. Jellison, Thin Solid Films **450**, 42 (2004).
[46] G. E. Jellison, Jr., C. O. Griffiths, and D. E. Holcomb, Appl. Phys. Lett. **81**, 1222 (2002).
[47] G. E. Jellison, L. A. Boatner, and C. Chen, Opt. Mater. (Amsterdam, Neth.) **15**, 103 (2000).
[48] J. Lee, P. I. Rovira, I. An, and R. W. Collins, Rev. Sci. Instrum. **69**, 1800 (1998).
[49] J. Lee, P. I. Rovira, I. An, and R. W. Collins, Appl. Phys. Lett. **72**, 900 (1998).
[50] P. I. Rovira, R. A. Yarussia, R. W. Collins, V. C. Venugopal, A. Lakhtakia, R. Messier, K. Robbie, and M. J. Brett, Thin Solid Films **313-314**, 373 (1998).
[51] A. S. Ferlauto, G. M. Ferreira, R. J. Koval, J. M. Pearce, C. R. Wronski, R. W. Collins, M. M. Al-Jassim, and K. M. Jones, Thin Solid Films **455-456**, 665 (2004).
[52] R. W. Collins, I. An, H. Fujiwara, J. Lee, Y. Lu, J. Koh, and P. I. Rovira, Thin Solid Films **313-314**, 18 (1998).
[53] C. Chen, I. An, G. M. Ferreira, N. J. Podraza, J. A. Zapien, and R. W. Collins, Thin Solid Films **455-456**, 14 (1998).
[54] J. Lee, J. Koh, and R. W. Collins, Rev. Sci. Instrum. **72**, 1742 (2001).
[55] R. W. Collins and J. Koh, J. Opt. Soc. Am. A **16**, 1997 (1999).
[56] C. Chen, I. An, and R. W. Collins, Phys. Rev. Lett. **90**, 217402 (2003).
[57] C. Chen, I. An, and R. W. Collins, Thin Solid Films **455-456**, 196 (2004).
[58] N. J. Podraza, C. Chen, I. An, G. M. Ferreira, P. I. Rovira, R. Messier, and R. W. Collins, Thin Solid Films **455-456**, 571 (2004).
[59] T. Girardeau, S. Camelio, D. Babonneau, J. Toudert, and A. Barranco, Thin Solid Films **455-456**, 313 (2004).
[60] M. Losurdo, D. Barreca, G. Bruno, and E. Tondello, Thin Solid Films **384**, 58 (2001).
[61] R. M. A. Azzam and N. M. Bashara, *Ellipsometry and Polarized Light* (North-Holland, Amsterdam, 1977).
[62] A. En Naciri, L. Broch, L. Johann, and R. Kleim, Thin Solid Films **406**, 103 (2002).
[63] C. D'Orléans, J. P. Stoquert, C. Estournès, J. J. Grob, D. Muller, C. Cerruti, and F. Haas, Nucl. Instrum. Methods Phys. Res. B **225**, 154 (2004).

[64] C. D'Orléans, J. P. Stoquert, C. Estournès, J. J. Grob, D. Muller, J. L. Guille, M. Richard-Plouet, C. Cerruti, and F. Haas, Nucl. Instrum. Methods Phys. Res. B **216**, 372 (2004).
[65] C. D'Orléans, J. P. Stoquert, C. Estournès, C. Cerruti, J. J. Grob, J. L. Guille, F. Haas, D. Muller, and M. Richard-Plouet, Phys. Rev. B **67**, 220101(R) (2003).
[66] M. Gilliot, A. En Naciri, L. Johann, J. P. Stoquert, J. J. Grob, and D. Muller, J. Appl. Phys. **101**, 014319 (2007).
[67] R. J. Gehr and R. W. Boyd, Chem. Mater. **8**, 1807 (1996).
[68] W. T. Doyle and I. S. Jacobs, J. Appl. Phys. **71**, 3926 (1992).
[69] J. A. Osborn, Phys. Rev. **67**, 351 (1945).
[70] L. Fu, P. B. Macedo, and L. Resca, Phys. Rev. B **47**, 13818 (1993).
[71] F. Claro and R. Rojas, Phys. Rev. B **43**, 6369 (1991).
[72] P. Yeh, *Optical Waves in Layered Media* (Wiley, New York, 1988).
[73] M. Schubert, Thin Solid Films **313-314**, 323 (1998).
[74] D. W. Berreman, J. Opt. Soc. Am. **62**, 502 (1972).
[75] M. Schubert, Phys. Rev. B **53**, 4265 (1996).
[76] J. Lekner, J. Phys.: Condens. Matter **3**, 6121 (1991).
[77] J. Lekner, Pure Appl. Opt. **3**, 821 (1994).
[78] J. Jackson, *Classical Electrodynamics* (Wiley, New York, 1999).
[79] N. Ashcroft and N. Mermin, *Solid State Physics* (Saunders, New York, 1988).
[80] C. Kittel, *Introduction to Solid State Physics* (Wiley, New York, 1996).
[81] J. Maxwell-Garnett, Philos. Trans. R. Soc. London, Ser. A **203**, 385 (1904).
[82] C. J. F. Böttcher, *Dielectrics in Static Fields*, Theory of Electric Polarization Vol. 1 (Elsevier, Amsterdam, 1973).